



Detection of lags in an atoll source 4U 1728-34 using AstroSat

P. Chiranjeevi¹ · K. Sriram¹ · S. Malu¹ · Vivek K. Agrawal²

Received: 3 July 2023 / Accepted: 13 September 2023 / Published online: 26 September 2023
© The Author(s), under exclusive licence to Springer Nature B.V. 2023

Abstract

Hard X-rays from atoll sources either can be emitted from the compact corona or the boundary layer around the neutron star surface. For the first time, we report the lags of the order of a few hundred seconds between soft and hard energy bands observed in an atoll source 4U 1728-34 using the AstroSat LAXPC data. We fitted the spectra with various models and found that the source was in the soft banana state during the observations and the inner disc radius was found to be ~ 16 km. Based on a thermal Comptonization model, the electron temperature was found to be low (~ 3 keV) with an index of $\Gamma = 1.82$, indicating that the corona was compact in nature. We noted that the boundary layer emission was relatively more than the disc emission component. Based on the reflection model, we noted that the inner disk front was at $R_{in} \sim 1.45 R_{ISCO}$ with an electron temperature ~ 2.72 keV. Based on the observed lags, the coronal height was estimated to be around 3-20 km assuming that the disc is close to the ISCO. We noted that the detected lags are similar to the depletion time scale of the boundary layer. These results indicate that the hard X-ray emission can arrive from the corona or boundary layer and the observed lags are due to readjustment time scales of either or both the physical structures.

Keywords Accretion · Accretion disc · Stars: neutron · X-rays: binaries · X-rays: individual · 4U 1728-34

1 Introduction

A neutron star (NS) that accretes matter from an evolved low-mass secondary star via Roche lobe overflow forms a low-mass X-ray binary (LMXB) system. NS LMXBs are classified into two categories: Atoll and Z-sources, based on the track in the X-ray colour-colour diagram (CCD) or hardness-intensity diagram (HID) (Hasinger and van der Klis 1989). In order to understand the fundamental physical changes in the source radiation, it is helpful to parameterize the spectral changes using CCDs and HIDs. Two branches—the island state (IS) and the banana branch—of the colour-colour diagram of atoll sources are typically visible. The banana branch is further divided into a lower banana (LB) and an upper banana (UB). Atoll source typically exhibits characteristics of the low/hard state which is associated with the island branch's low mass accretion rate. It is widely accepted that the accretion disc is truncated in this condition

at quite a distance from the compact object. The atoll source moves from the island to the banana state as the mass accretion rate increases. During this state, atoll source spectra generally show soft state characteristics, and the accretion disc is believed to be approaching the compact object. The corona temperature typically decreases as the source transitions from an island to a banana state, while thermal emission in the form of blackbody/disc blackbody typically increases (van der Klis 1995). An atoll source moves from IS to UB followed by an increase in brightness, which typically indicates an increase in the accretion rate. Atoll sources exhibit luminosities lower than Z sources ($0.001 - 0.5 L_{Edd}$), have weaker magnetic fields of $B \sim 10^8$ G, and relatively less spectral variability. They take a few hours to days to move along the banana branch while traversing along the island state requires a few days to weeks.

Quasi Periodic Oscillations (QPOs) in the power density spectra, which are usually associated with specific locations on the CCD/HID, are one of the temporal variability characteristics of Atoll sources (Hasinger and van der Klis 1989). When an atoll source moves along its CCD/HID, almost all the timing features defining the power density spectra of these sources appear to change in a smooth and monotonic manner (Psaltis et al. 1999; Wijnands and van der Klis 1999), implying a close relationship between spectral and

✉ P. Chiranjeevi

¹ Department of Astronomy, Osmania University, Hyderabad, 500007, India

² Space Astronomy Group, U R Rao Satellite Center, ISITE Campus, Bangalore, 560037, India

temporal behavior (van der Klis 2004). QPOs are typically seen in atoll sources in the millihertz to kilohertz frequency range. In the island state and lower banana branch, kilohertz QPOs or twin kHz QPOs in the frequency region of 300–1200 Hz are frequently seen (van der Klis 2004).

4U 1728-34 is an Atoll-type low-mass X-ray binary with an evolved, hydrogen-poor donor star (Shaposhnikov et al. 2003). This binary's compact object is a weakly magnetised accreting NS, and its optical counterpart has not yet been detected. This source has produced a type-I X-ray burst as well as a double-peaked burst profile (Basinska et al. 1984; Hoffman et al. 1976). Helium-rich bursts are indicated by Type-I burst morphology (Galloway et al. 2008). Several attempts have been made using the Eddington luminosity of burst profile to confine the distance of the source in the range 4.1-5.1 kpc (Di Salvo et al. 2000; Galloway et al. 2003; Shaposhnikov et al. 2003). The source also exhibited kilohertz quasi-periodic oscillations (kHz QPO's) in the persistent emission, as well as a nearly coherent oscillation at 363 Hz (Strohmayer et al. 1996), which has been proposed as the NS spin frequency.

Based on RXTE and INTEGRAL spectra, Tarana et al. (2011) showed that the soft spectra exhibited by 4U 1728-34 are characterized by a prominent black body emission along with a Comptonized component whereas hard spectra are excessively Comptonized and non-thermal emission dominates the high energy band. Several spectral studies of 4U 1728-34 with satellites including, XMM-Newton (Ng et al. 2010; Egron et al. 2011), BeppoSAX (Di Salvo et al. 2000; Piraino et al. 2000; Seifina and Titarchuk 2011), and RXTE (Piraino et al. 2000; Seifina and Titarchuk 2011) have found a broad emission line at 6.7 keV. Based on AstroSat data Verdhan Chauhan et al. (2017) found that the spectra can be well described with a pure thermal Comptonization model having a photon index of ~ 1.8 and a low-temperature corona $kT_e \sim 3$ keV. Based on NuSTAR and SWIFT data, Sleanor et al. (2016) reported a low disc truncation radius i.e. $\leq 2 R_g$ whereas Mondal et al. (2017) higher inner radius of 2.3 and 3.7 R_{ISCO} in soft and hard states respectively. Based on XMM-Newton and RXTE joint spectral fits, Wang et al. (2019) observed that the inner disc radius decreased as the atoll source traversed from a soft to a hard state with $R_{in} = 1.9-3.7 R_{ISCO}$ during soft states. It was observed that the continuum spectra were dominated by the illumination of the disc due to the corona than the boundary layer emission.

Cross-Correlation Function (CCF) studies have been previously reported for various Z and atoll sources. A similar study by Lei et al. (2008) using soft and hard energy bands of 2-5 keV vs. 16-30 keV, for Cyg X-2, which is a Z source, showed a few hundred seconds of soft and hard lags. Their study associated the anticorrelated lags that were found in the HB and NB with low mass accretion rates. CCF studies on atoll sources 4U 1735-44 and 4U 1608-52 (Lei et al.

2013, 2014) similarly revealed a few 10-100 s lags when atoll sources were in both banana and island states. Malu et al. (2021b,a) studied detected hard and soft lags in an atoll source 4U 1705-44 based on Astrosat data and interpreted the lags to be readjustment timescale of the corona or boundary layer. The Z source GX 5-1 gave lags of similar order (Sriram et al. 2012) which were then attributed to a truncated accretion disk-corona geometry. But studies by Sriram et al. (2019) on Z source GX 17+2 yet again showed a few hundred seconds lag when the source was in the HB and NB, even when the disc was found to be close to the ISCO. This, in effect, can lead to the conclusion that a disc variation might not be the possible cause of lags. Both correlated and anticorrelated lags were noticed in these branches, whereas highly correlated CCFs with $CC > 0.8$ were noticed in the FB. This indirectly indicated a possible connection between the origin of CCFs and jet emission. It was found during this study that the readjustment of the corona or hard X-ray emitting region could be the primary contributor to the obtained CCF lags, which gave a measure for coronal heights. For the atoll source 4U 1705-44, using the much softer 0.8-3 keV energy band and 10-20 keV hard energy band (Malu et al. 2021b), CCF studies were performed to distinctly study the coronal and disc variations. Lags of 38 to 259 s were found in these studies as well.

2 LAXPC data reduction

The AstroSat archival data from Large Area X-ray Proportional Counter (LAXPC) the source 4U 1728-34 with the Observation ID of the data set T01_041T01_9000000362 starting from 2016, March 07 to 2016, March 09 were used for timing and spectral analysis. The combined effective area of three co-aligned identical proportional counters (LAXPC10, LAXPC20, and LAXPC30) at 15 keV is approximately 6000 cm² (Yadav et al. 2016; Agrawal et al. 2017; Antia et al. 2017). The background and spectral response were produced as described in Antia et al. (2017). We reduced LAXPC level 1 data to level 2 data using the LAXPC software (Format A, Aug 04, 2020 version)¹ provided by the AstroSat Support Center (ASSC). LAXPC10 data has been used for timing and spectral analysis.

3 Timing analysis

The LAXPC 3.0-20.0 keV light curve is shown in Fig. 1 left panel displays a few bursts and the right panel shows the same without the bursts. The hardness intensity diagram (HID) was obtained, (Fig. 2), where the hard colour is defined

¹<http://Astrosat-ssc.iucaa.in/?q=laxpcData>.

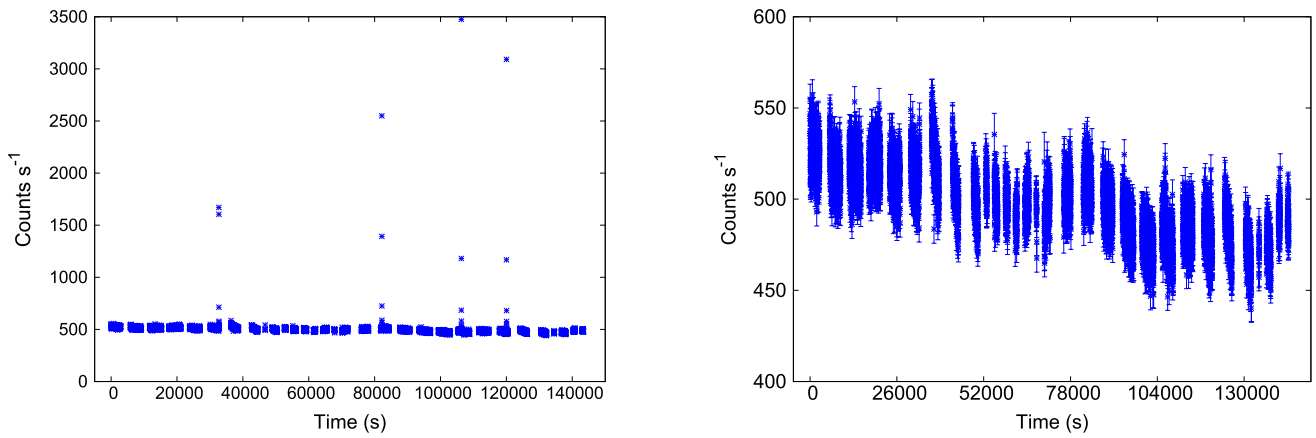
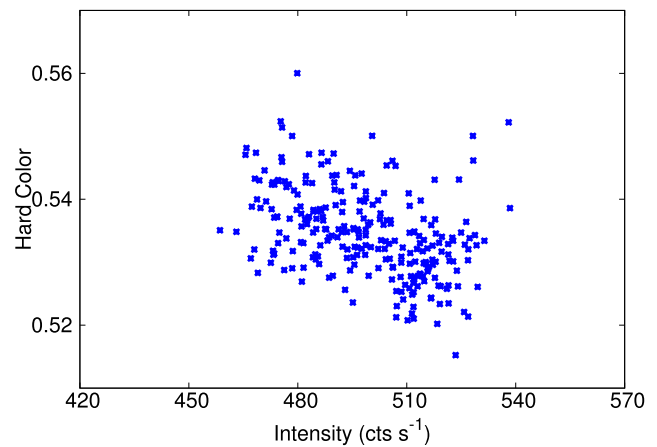


Fig. 1 Left panel: Background subtracted light curve in 3.0-20.0 keV range with 8 s bin. The right panel shows the same without the bursts

Fig. 2 The Hardness Intensity Diagram (HID) of 4U 1728-34 observed with AstroSat LAXPC 10 data. Hard colour is defined as 8.0-20.0/3.0-8.0 keV and intensity is in the energy band of 3.0-20.0 keV with a bin time of 256 s



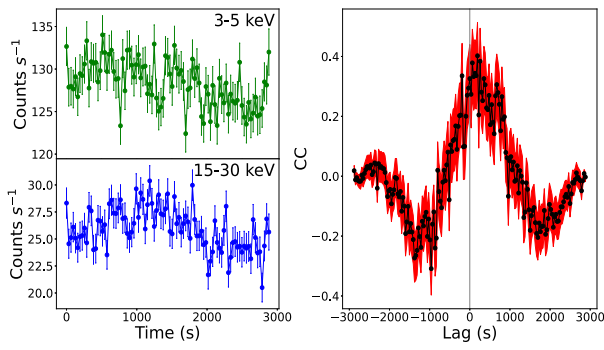
as the ratio between 8.0-20.0 keV and 3.0-8.0 keV and intensity was measured in the energy range of 3.0-20.0 keV. For the first time, we performed the Cross-Correlation Functions (CCF) of 4U 1728-34, between soft (3-5 keV) and hard (15-30 keV) energy band light curves using the AstroSat data. The exposure times and obtained CCF information of each orbit is displayed in Table 1. Crosscor, a program included in the XRONOS package, was used to obtain the CCF with a bin time of 32 s (Sriram et al. 2007, 2021). Figure 3 shows the soft and hard light curves (top and bottom panels on the left) and the corresponding CCFs in the right panels. A vertical line in each figure denotes zero lag and the shaded region (red) represents the CCF standard deviation. Table 1 lists each correlation coefficient (CC), lag, and associated error bar. CCFs were fitted with a Gaussian function, and errors were calculated using the criteria of $\Delta\chi^2 = 2.71$ at a 90% confidence level.

It was clear that there is a strong asymmetry in the CCF profiles, strongly indicating the presence of lags. Between the 3-5 keV and 15-30 keV energy bands, orbit 02393 exhibited a positively correlated hard lag of 252 ± 70 s. In orbit 02396, no significant lag viz. -37 ± 33 s was detected

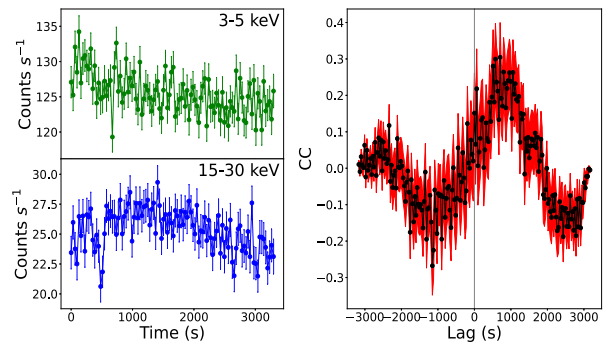
Table 1 Log of the observations and the corresponding detected Lags in 4U 1728-34 using the AstroSat LAXPC 10 data. Here 02415(22) and 02415(23) are the 22nd and 23rd segments of the light curve displayed in Fig. 1

| Orbit | Exposure time (s) | 3-5 vs 15-30 keV | |
|-----------|-------------------|------------------|---------------|
| | | CC | Lag (s) |
| 02393 | 2904 | 0.31 ± 0.05 | 252 ± 70 |
| 02394 | 3326 | 0.23 ± 0.04 | 817 ± 86 |
| 02396 | 3586 | 0.47 ± 0.05 | -37 ± 33 |
| 02407 | 2092 | 0.36 ± 0.05 | 138 ± 44 |
| 02408 | 3016 | 0.27 ± 0.04 | 470 ± 103 |
| 02415(22) | 3620 | 0.21 ± 0.04 | 424 ± 105 |
| 02415(23) | 3484 | 0.18 ± 0.04 | 331 ± 90 |

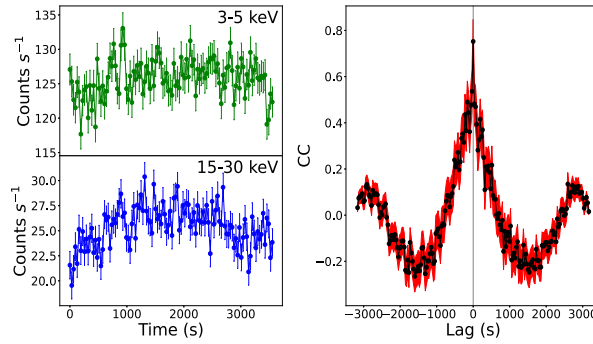
and CCF was positively correlated. The remaining CCF information is provided in Table 1 and shown in Fig. 3. It has been noted that detected lags are positively correlated. We assume that the observed lags are readjustment time scales of the inner region of the accretion disc producing the soft and hard photons, where the Comptonization structure or



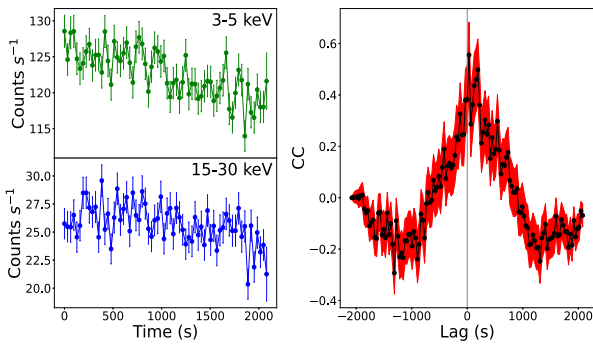
(a) 02393



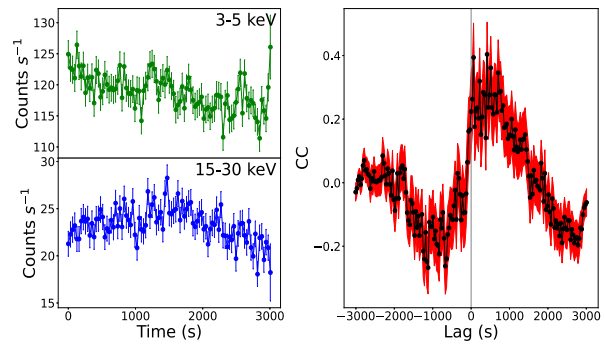
(b) 02394



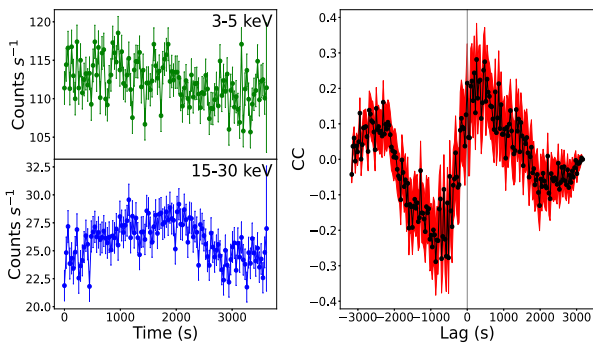
(c) 02396



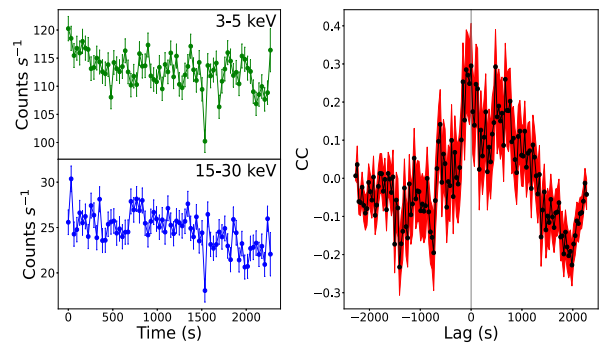
(d) 02407



(e) 02408



(f) 02415(22)



(g) 02415(23)

Fig. 3 The background-subtracted LAXPC soft (3–5 keV) and hard (15–30 keV) light curves the left side in the figure, and the right side shows the corresponding cross-correlation function. Energy bands are

mentioned in the light curves. Shaded regions show the standard deviation of the CCFs

boundary layer is potentially changing in its size, based on our previous studies (Sriram et al. 2012, 2019; Malu et al. 2021b; Sriram et al. 2021; Chiranjeevi and Sriram 2022).

4 Spectral analysis

In order to constrain the parameter responsible for causing the lags, we performed spectral analysis for all the orbits. We used LAXPC 10 data for spectral analysis for all orbits. Various multicomponent models were used to unfold the spectra in the 3–25 keV energy band which incorporates both soft and hard components. First, we fitted a two-component model viz. $tbabs*(bbody+gaussian+cutoffpl)$. The hydrogen column density N_H was fixed at $2.3 \times 10^{22} \text{ cm}^{-2}$ (Galloway et al. 2010; Bhattacharyya et al. 2018) along with Fe line at 6.7 keV (Fig. 4, Table 2). When fitting spectra, a systematic error of 2% was included (Bhattacharyya

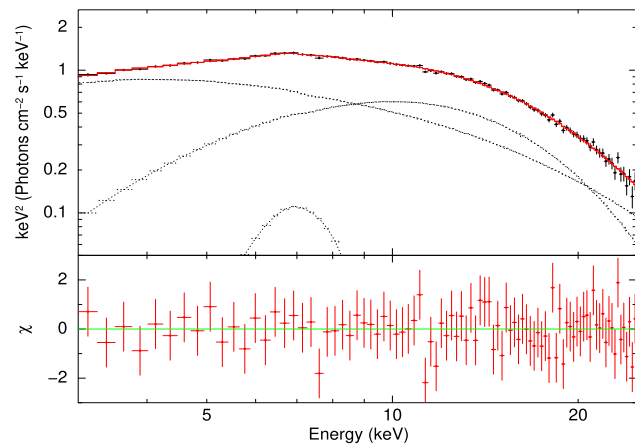


Fig. 4 Unfolded Spectrum for the model $tbabs*(bbody+gaussian+cutoffpl)$ for the orbit 02393 in the 3.0-25.0 keV range

Table 2 Best-fit parameters of the spectra of different segments using the model $tbabs*(bbody+gaussian+cutoffpl)$. N_H is $2.3 \times 10^{22} \text{ cm}^{-2}$ fixed absorption column density. kT_{bb} is the bbody temperature. N_{bb} is the normalization of the bbody component. Γ is the power law photon

| Parameter | 02393 | 02394 | 02396 | 02407 | 02408 | 02415(22) | 02415(23) |
|-----------------------|---------------------------|---------------------------|---------------------------|---------------------------|---------------------------|---------------------------|---------------------------|
| kT_{bb} (keV) | $2.50^{+0.12}_{-0.09}$ | $2.61^{+0.16}_{-0.12}$ | $2.61^{+0.12}_{-0.10}$ | $2.48^{+0.13}_{-0.09}$ | $2.53^{+0.14}_{-0.10}$ | $2.70^{+0.19}_{-0.15}$ | $2.55^{+0.14}_{-0.10}$ |
| N_{bb} | $0.016^{+0.002}_{-0.002}$ | $0.014^{+0.002}_{-0.002}$ | $0.016^{+0.002}_{-0.002}$ | $0.014^{+0.001}_{-0.002}$ | $0.013^{+0.001}_{-0.002}$ | $0.011^{+0.001}_{-0.002}$ | $0.012^{+0.001}_{-0.002}$ |
| Γ | $1.94^{+0.30}_{-0.30}$ | $1.83^{+0.30}_{-0.34}$ | $1.89^{+0.30}_{-0.38}$ | $2.02^{+0.28}_{-0.28}$ | $2.03^{+0.28}_{-0.29}$ | $1.91^{+0.28}_{-0.28}$ | $2.00^{+0.28}_{-0.28}$ |
| E_{cpl} (keV) | $8.46^{+3.21}_{-2.06}$ | $7.21^{+2.63}_{-2.51}$ | $7.00^{+2.7}_{-2.81}$ | $9.93^{+4.20}_{-2.43}$ | $9.67^{+4.08}_{-2.49}$ | $9.22^{+3.69}_{-2.51}$ | $10.66^{+4.70}_{-2.62}$ |
| N_{cpl} | $1.51^{+0.46}_{-0.35}$ | $1.41^{+0.41}_{-0.31}$ | $1.52^{+0.44}_{-0.34}$ | $1.59^{+0.46}_{-0.35}$ | $1.54^{+0.44}_{-0.34}$ | $1.28^{+0.36}_{-0.27}$ | $1.38^{+0.40}_{-0.31}$ |
| Flux _{bb} | 1.26 | 1.16 | 1.29 | 1.13 | 1.08 | 1.90 | 1.97 |
| Flux _{cpl} | 2.05 | 2.03 | 1.93 | 2.13 | 1.99 | 2.01 | 2.04 |
| Flux _{total} | 3.38 | 3.28 | 3.31 | 3.33 | 3.15 | 3.01 | 3.10 |
| χ^2/dof | 50/84 | 67/84 | 58/84 | 50/84 | 58/84 | 59/84 | 71/84 |

et al. 2018). The $\Delta\chi^2/\text{dof}$ values for orbits 02393, 02394, and 02396 are 50/84, 67/84, 58/84, 50/84, 58/84, 59/84 and 71/84 respectively. kT_{bb} was found to be around 2.50 keV and was not observed to be varying in other orbits. The cut-off power-law index was noted to be $\Gamma \sim 1.90$ associated with a low cut-off energy $E_{cpl} \sim 9 \text{ keV}$ for all the orbits. Overall $bbody$, $Gaussian$, and $cutoffpl$ parameters in all the orbits did not exhibit any appreciable deviations. Our study reveals that a low temperature optically thick corona is a characteristic of the Comptonization area. The total unabsorbed flux was found to be around $3.3 \times 10^{-9} \text{ erg cm}^{-2} \text{ s}^{-1}$ (Table 2).

Verdhan Chauhan et al. (2017) fitted the spectrum of the source using the thermal Comptonization model. We also used the model i.e. $tbabs*(nthcomp+gaussian)$ to unfold the spectra. We used both blackbody and disc soft seed photons configuration in the nthcomp model and found no significant difference in the spectral parameters (Table 3, Fig. 5). The asymptotic power-law index was found to be at $\Gamma \sim 1.8$ with an electron temperature of the corona $kT_e \sim 3.1 \text{ keV}$. It is clear that a low-temperature corona can explain the banana state. Overall from the above spectral analysis, the corona/bbody structure varies during the detected lags.

5 Results and discussion

For the first time, we used AstroSat’s energy dependent light curves to estimate the lags between soft and hard energy bands of 4U 1728-34. We found both soft and hard lags of the order of a few hundred seconds when the atoll source was in a banana state. Such lags were previously observed in atoll sources viz. 4U 1735-44 and 4U 1608-52 (Lei et al. 2013, 2014) and interpreted as the movement of the inner

index. E_{cpl} is the e-folding energy of exponential roll-off. N_{cpl} is the normalization of cutoffpl. Iron line fixed at 6.7 keV. Flux is in units of $10^{-9} \text{ erg cm}^{-2} \text{ s}^{-1}$

Table 3 Best-fit parameters of the spectra of different segments using the model $tbabs*(nthcomp+gaussian)$. N_H is $2.3 \times 10^{22} \text{ cm}^{-2}$ fixed absorption column density. Γ is the $nthcomp$ power-law photon index. kT_e is the electron temperature. Iron line fixed at 6.7 keV. N_{nth} is the normalization for $nthcomp$. Flux is in units of $10^{-9} \text{ erg cm}^{-2} \text{ s}^{-1}$

| Parameter | blackbody | | | | | | |
|--------------------------|------------------------|------------------------|------------------------|-------------------------|------------------------|------------------------|------------------------|
| | 02393 | 02394 | 02396 | 02407 | 02408 | 02415(22) | 02415(23) |
| Γ | $1.82^{+0.01}_{-0.01}$ | $1.85^{+0.01}_{-0.01}$ | $1.83^{+0.01}_{-0.01}$ | $1.86^{+0.01}_{-0.007}$ | $1.86^{+0.01}_{-0.01}$ | $1.88^{+0.01}_{-0.01}$ | $1.87^{+0.01}_{-0.01}$ |
| kT_e (keV) | $3.06^{+0.04}_{-0.04}$ | $3.12^{+0.04}_{-0.04}$ | $3.07^{+0.03}_{-0.03}$ | $3.16^{+0.04}_{-0.04}$ | $3.17^{+0.04}_{-0.04}$ | $3.37^{+0.04}_{-0.04}$ | $3.28^{+0.04}_{-0.04}$ |
| N_{nth} | $0.85^{+0.03}_{-0.02}$ | $0.86^{+0.03}_{-0.03}$ | $0.84^{+0.01}_{-0.02}$ | $0.81^{+0.03}_{-0.03}$ | $0.81^{+0.03}_{-0.03}$ | $0.75^{+0.04}_{-0.04}$ | $0.74^{+0.03}_{-0.03}$ |
| Flux $_{nth}$ | 3.35 | 3.24 | 3.28 | 3.31 | 3.11 | 2.98 | 3.07 |
| cutoffpl Flux $_{total}$ | 3.38 | 3.28 | 3.31 | 3.33 | 3.15 | 3.01 | 3.10 |
| χ^2/dof | 60/86 | 74/86 | 72/86 | 65/86 | 73/86 | 82/86 | 73/86 |
| Parameter | disc blackbody | | | | | | |
| | 02393 | 02394 | 02396 | 02407 | 02408 | 02415(22) | 02415(23) |
| Γ | $1.82^{+0.01}_{-0.01}$ | $1.85^{+0.01}_{-0.01}$ | $1.83^{+0.01}_{-0.01}$ | $1.86^{+0.01}_{-0.01}$ | $1.86^{+0.01}_{-0.01}$ | $1.87^{+0.01}_{-0.01}$ | $1.87^{+0.01}_{-0.01}$ |
| kT_e (keV) | $3.06^{+0.04}_{-0.04}$ | $3.12^{+0.04}_{-0.04}$ | $3.07^{+0.03}_{-0.03}$ | $3.16^{+0.04}_{-0.03}$ | $3.17^{+0.04}_{-0.04}$ | $3.35^{+0.03}_{-0.04}$ | $3.28^{+0.02}_{-0.04}$ |
| N_{nth} | $0.92^{+0.03}_{-0.03}$ | $0.93^{+0.03}_{-0.03}$ | $0.90^{+0.03}_{-0.03}$ | $1.00^{+0.03}_{-0.03}$ | $0.93^{+0.03}_{-0.03}$ | $0.90^{+0.03}_{-0.03}$ | $0.91^{+0.03}_{-0.03}$ |
| Flux $_{nth}$ | 3.35 | 3.24 | 3.28 | 3.31 | 3.13 | 2.98 | 3.07 |
| cutoffpl Flux $_{total}$ | 3.38 | 3.28 | 3.31 | 3.33 | 3.15 | 3.01 | 3.10 |
| χ^2/dof | 60/86 | 74/86 | 72/86 | 65/86 | 73/86 | 82/86 | 73/86 |

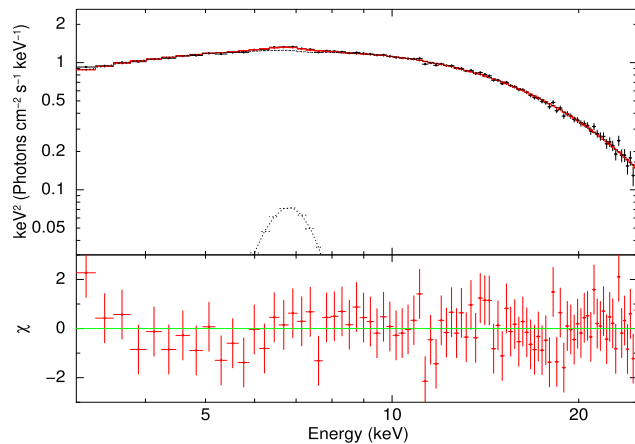


Fig. 5 Unfolded Spectrum for the model $tbabs*(nthcom+gaussian)$ for the orbit 02393 in the 3.0–25.0 keV range

front of the disc, supporting the truncated disc model. Similarly, such lags were also observed in Z source viz. GX 5-1, GX 17+2 etc. (Sriram et al. 2012, 2019, 2021; Chiranjeevi and Sriram 2022). In an orbit 02396, we observed positively correlated CCF with an insignificant lag of -37 ± 33 s. Previous studies in Z and atoll sources (Sriram et al. 2012; Lei et al. 2013, 2014; Sriram et al. 2019), it was observed that during similar spectral some CCFs are well correlated and some display lags. We suggest that during the lags the inner accretion disk structure is changing. Later, based on detailed

timing and spectral studies of an atoll source 4U1705-44, Malu et al. (2021b,a) showed that the inner disc radius was not varying during the detected lags and was found to be close to the last stable orbit. It was suggested that the lags were associated with the structural variation of the boundary layer or the corona or could be both. We performed a simulation in order to verify the significance of the observed lags. The significance of the CCFs was determined by following a probabilistic approach similar to that of Maoz and Netzer (1989). The flux of the light curves was randomly redistributed 1000 times, where after each redistribution CCF lags and CCs were determined. This results in a Cross-Correlation Probability Distribution of the obtained lags. The centroid value of this distribution was computed by fitting a Gaussian model to the distribution, giving the final time lag between the two light curves where the corresponding standard deviation is the lag uncertainty. The lag obtained was 796 ± 164 s for orbit 02394, which is correlated and hard. A correlated hard lag of 450 ± 220 s was obtained for orbit 02408 (Fig. 6).

Generally, in the banana state, the source spectrum is soft with a smaller contribution from the corona. Moreover, since the disc is closer to the NS surface, the material accreting onto the surface decelerates and forms a boundary layer which also contributes to the spectra in the energy domain of 5–20 keV (Gilfanov et al. 2003; Revnivtsev and Gilfanov 2006). It is difficult to constrain how much the corona and boundary layer contribute to the X-ray spectrum. Wang

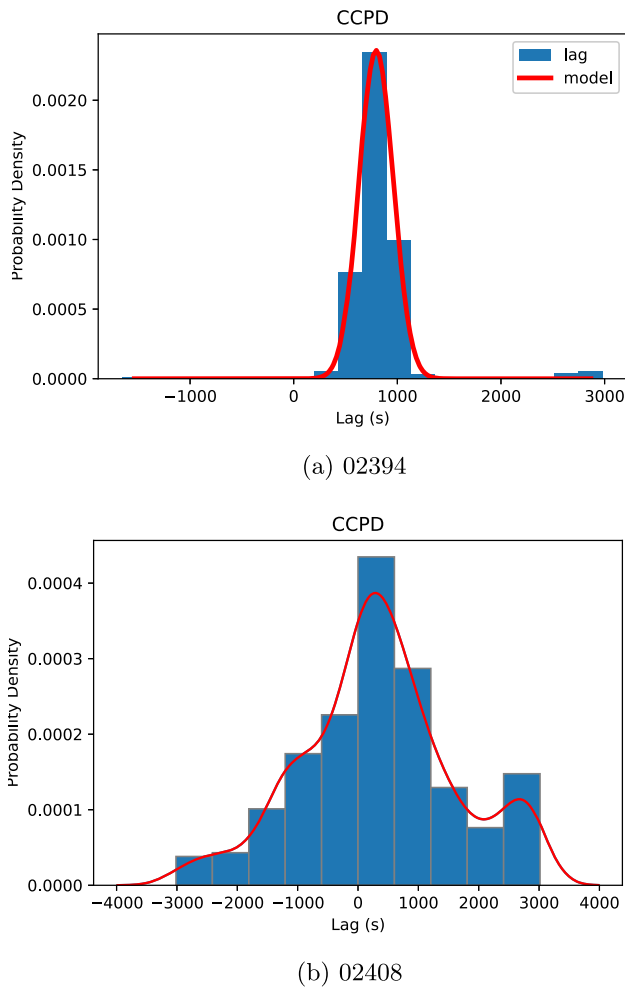


Fig. 6 CCPD distribution obtained from the simulations (see text) for the orbits 02394 and 02408. The red line displays the Gaussian fit to the peak of the CCPD

et al. (2019) observed that the reflection component of the X-ray spectra of 4U 1728-34 observed from XMM-Newton

is suitably described by both the corona and boundary layer, but the former component is dominant in explaining the reflection component of the spectra. We noted hard and soft lags which possibly arise either due to the boundary layer or corona or both and the respective lags cannot be decoupled as both the components contribute to the spectra. It is quite possible that the observed lags are caused by the readjustment of the boundary layer due to different radiative and dynamical configurations attained around the NS surface. Babkovskaia et al. (2008) studied the gas flow in the close vicinity of the neutron star and noted that the radiation pressure and centrifugal force at higher latitudes played a more pivotal role than the gravitational force. It was observed the material is accreted at higher latitudes and excreting at the equator. Hence, there is a velocity gradient from the equator to the higher latitudes, and any variation in the gradient will change the structure of the boundary layer.

We noted the bbody temperature to be $kT_{bb} \sim 2.5$ keV and low energy cutoff energy around $E_{cpl} \sim 8$ keV (Table 2) suggesting that the source was in a soft state which has often been observed in the source based on RXTE and INTEGRAL data (Tarana et al. 2011). In general, the thermal component is dominant in the soft state, and the emission is probably dominated by both the Keplerian portion of the disc depending on the disc radius [$T(R) \propto R^{-3/4}$] and NS boundary layer. However, it is not easy to distinguish from the observed spectra. We also invoked a pure thermal multi-component model for the soft state i.e. bbody+diskbb based on the studies of Tarana et al. (2011). We noted that this model resulted in reasonable fits (see Table 4). The inner disc temperature was around $kT_{in} \sim 1.28$ keV along with a normalization $N_{dbb} = 55.17^{+17.90}_{-14.30}$ for orbit 02393.

The inner disc radius calculated from the formula R_{in} (km) = $\sqrt{(N/\cos i)} \times D/10$ kpc, by considering $i = 50^\circ$ (Shaposhnikov et al. 2003; Wang et al. 2019) and distance $D = 5$ kpc (Shaposhnikov et al. 2003) to be $4.63^{+0.69}_{-0.64}$ km. The estimated radius is not the true radius

Table 4 Best-fit parameters of the spectra of different segments using the model $tbabs*(diskbb+gaussian+bbody)$. N_H is $2.3 \times 10^{22} \text{ cm}^{-2}$ fixed absorption column density. kT_{in} is the diskbb temperature. N_{dbb}

is the normalization of the diskbb component. kT_{bb} is the bbody temperature. N_{bb} is the normalization of the bbody component. Iron line fixed at 6.7 keV. Flux is in units of $10^{-9} \text{ erg cm}^{-2} \text{ s}^{-1}$

| Parameter | 02393 | 02394 | 02396 | 02407 | 02408 | 02415(22) | 02415(23) |
|-----------------------|-----------------------------|-----------------------------|-----------------------------|-----------------------------|-----------------------------|-----------------------------|-----------------------------|
| kT_{in} (keV) | $1.28^{+0.09}_{-0.07}$ | $1.29^{+0.08}_{-0.07}$ | $1.23^{+0.07}_{-0.06}$ | $1.32^{+0.09}_{-0.08}$ | $1.29^{+0.08}_{-0.07}$ | $1.33^{+0.08}_{-0.07}$ | $1.36^{+0.08}_{-0.06}$ |
| N_{dbb} | $55.17^{+17.90}_{-14.30}$ | $53.45^{+16.50}_{-13.22}$ | $64.50^{+19.12}_{-15.44}$ | $49.52^{+15.85}_{-12.58}$ | $51.86^{+16.04}_{-12.90}$ | $41.84^{+12.88}_{-10.35}$ | $39.85^{+14.67}_{-11.82}$ |
| kT_{bb} (keV) | $2.64^{+0.04}_{-0.03}$ | $2.68^{+0.04}_{-0.03}$ | $2.63^{+0.02}_{-0.02}$ | $2.74^{+0.05}_{-0.04}$ | $2.73^{+0.05}_{-0.04}$ | $2.86^{+0.04}_{-0.03}$ | $2.83^{+0.03}_{-0.02}$ |
| N_{bb} | $0.024^{+0.0009}_{-0.0007}$ | $0.023^{+0.0007}_{-0.0009}$ | $0.024^{+0.0005}_{-0.0006}$ | $0.027^{+0.0009}_{-0.0011}$ | $0.022^{+0.0007}_{-0.0009}$ | $0.020^{+0.0005}_{-0.0006}$ | $0.024^{+0.0004}_{-0.0005}$ |
| Flux _{dbb} | 1.21 | 1.21 | 1.15 | 1.29 | 1.19 | 1.16 | 1.21 |
| Flux _{bb} | 1.96 | 1.84 | 1.96 | 1.79 | 1.73 | 1.61 | 1.65 |
| Flux _{total} | 3.38 | 3.28 | 3.31 | 3.33 | 3.15 | 3.01 | 3.10 |
| χ^2/dof | 77/85 | 84/85 | 73/85 | 81/85 | 87/85 | 87/85 | 81/85 |

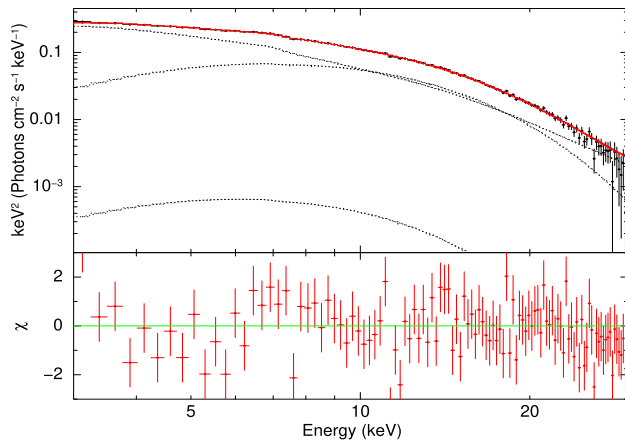


Fig. 7 Unfolded Spectrum for the model $tbabs*(bbodyrad+relxillcp+nthcomp)$ for the orbit 02393

and should be corrected by the spectral hardening factor ($\kappa \sim 1.7\text{--}2.0$; Shimura and Takahara (1995)) together with the internal boundary condition correction factor ($\zeta = 0.41$; Kubota et al. (1998)). The effective radius R_{eff} is 1.18–1.64 times the true radius value ($R_{eff} = \kappa^2 \zeta R_{in}$ Kubota et al. (2001)). After correction, the inner disc radius was determined to be $5.48^{+0.82}_{-0.76}$ km – $7.59^{+1.14}_{-1.05}$ km.

These R_{in} values indicate that during this state the source inner disc was close to the neutron star’s surface. We also found that the bbody flux is relatively higher which could indicate that most of the emission is arriving from the boundary layer. The structure of the corona during the soft is not adequately known but is generally assumed to be cool, optically thick, and compact. We attempted a pure comptonization model based on Verdhan Chauhan et al. (2017) which resulted in good fits. We noted a low electron temperature $kT_e = 3.1$ keV.

The previous spectrum exhibited by 4U 1728–34 was fitted with a reflection model (Wang et al. 2019), where the keplerian portion of the disc is illuminated by a continuum power-law source i.e. corona located over the disk. Hence, we also unfolded the spectra using RELXILLCP2 v2.2 (García et al. 2014; Dauser et al. 2016) shown in Fig. 7. The overall model invoked was $tbabs*(bbodyrad+relxillcp+nthcomp)$ where $N_H = 2.3 \times 10^{22}$ cm², $a_* = 0.17$ (Wang et al. 2019), and $R_{out} = 1000 R_g$ were fixed. We tied $q_{in} = q_{out}$ and electron temperature kT_e of relxillcp and nthcomp model were tied. The use of nthcomp model and tying of the parameter provides the individual flux components (Wang et al. 2019). The best-fit results are displayed in Table 5 with $\chi^2/dof = 123/109$. We noted that $kT_{bb} = 2.04$ keV, inner disc radius $R_{in} = 1.45 \pm 0.17 R_{ISCO}$ along with the continuum illuminating power-law source with index $\Gamma = 1.78 \pm 0.003$. It is observed that the R_{in} is found to be different when estimated from diskbb normalization and reflection model which is about 16 km. Since the

Table 5 Best-fit parameters of the spectra of different segments using the model $tbabs*(bbodyrad+relxillcp+nthcomp)$. N_H is 2.3×10^{22} cm^{−2} fixed absorption column density. Flux is in units of 10^{-9} erg cm^{−2} s^{−1}

| | Parameter | 02393 |
|-----------|---|------------------------------|
| bbodyrad | kT_{bb} (keV) | $2.04^{+0.03}_{-0.02}$ |
| | N_{bb} (km ² /100 kpc ²) | $0.054^{+0.14}_{-0.15}$ |
| | q_{in} (keV) | $3.0^{+0.30}_{-0.25}$ |
| | A_{Fe} (keV) | $3.37^{+0.68}_{-0.42}$ |
| | i (°) | $38.91^{+2.17}_{-5.30}$ |
| relxillcp | a_* | 0.17 (fix) |
| | kT_e (keV) | $2.72^{+0.32}_{-0.42}$ |
| | Γ | $1.78^{+0.13}_{-0.18}$ |
| | R_{in} (R_{ISCO}) | $1.45^{+0.18}_{-0.26}$ |
| | $\text{Log } \zeta$ (erg cms ^{−1}) | $2.99^{+0.038}_{-0.045}$ |
| | refl_frac | $0.89^{+0.023}_{-0.033}$ |
| nthcomp | N_{relp} (10^{-3}) | $4.28^{+0.04}_{-0.02}$ |
| | N_{nth} | $0.0065^{+0.0001}_{-0.0001}$ |
| | Flux _{total} | 3.43 |
| | χ^2/dof | 123/109 |

reflection model better describes the spectrum, we suggest that the disk is slightly truncated but we caution the reader that more observations are needed to confirm the location of the inner region of the disk in the respective spectral state.

Overall we concluded that the inner disc radius was slightly away from the last stable orbit similar to the results obtained by Wang et al. (2019) where they found $R_{in} = 1.9 \pm 0.20 R_{ISCO}$.

Based on Swift+NuStar data analysis, it was found that as the 4U 1728–34 traversed from hard to soft state, the inner disc radii were noted to be $3.7^{+2.2}_{-0.7}$ and $2.3^{+2.1}_{-1.0} R_{ISCO}$ suggesting that it remained constant (Mondal et al. 2017). However, Wang et al. (2019) observed that the inner disc radius varied, in fact, increased when the source evolved from a hard to a soft state based on the XMM-Newton and RXTE spectra. This is contrary to the standard accretion theory since, as the mass accretion rate increases from hard to soft state the inner disc front must move closer to the NS surface thereby decreasing the truncation radius. They explained the higher radius in the soft state using the higher radiation pressure experienced by the disc at higher X-ray luminosities.

5.1 Coronal height estimation

Since the inner disc radius is located close to the NS surface and assuming that the detected lags are due to variation in the corona, we can estimate the coronal height us-

ing the equation given by Sriram et al. (2019). We interpret the lags as the readjustment time scales during which the corona structure is varying. The following equation was used to limit the coronal size (Shakura and Sunyaev 1973; Sriram et al. 2019).

$$H_{corona} = \left(\frac{t_{lag} \dot{m}}{2\pi R_{disk} H_{disk} \rho} - R_{disk} \right) \times \beta \text{ cm} \tag{1}$$

Here is

$$H_{disk} = 10^8 \alpha^{-1/10} \dot{m}_{16}^{3/20} R_{10}^{9/8} f^{3/20} \text{ cm}$$

$$\rho = 7 \times 10^{-8} \alpha^{-7/10} \dot{m}_{16}^{11/20} R_{10}^{-15/8} f^{11/20} \text{ g cm}^{-3}$$

$$f = (1 - (R_s/R)^{1/2})^{1/4}$$

and

$$\beta = v_{corona}/v_{disk}$$

Assuming a $\beta = 0.01, 0.05$ and 0.1 (Manmoto et al. 1997; Pen et al. 2003; McKinney et al. 2012) and mass of NS to be $1.4 M_{\odot}$, R_{ISCO} can be approximated as $R_{ISCO} \simeq (6GM/C^2)(1 - 0.54a_*)$ (van der Klis 2000; Mondal et al. 2017). Here $a_* = 0.17$ is the neutron star spin for 4U 1728-34, therefore $R_{ISCO} = 11.26$ km, and thus the inner accretion disc radius $R_{in} = 1.45 \times 11.26$ km = 16.32 km.

Here we calculated $\dot{m} = 5.28 \times 10^{17} \text{ g s}^{-1}$ using the relation $L = GM\dot{m}/R_N \text{ ergs s}^{-1}$, with M being the neutron star mass, R_N the neutron star radius $R_N = 10$ km and $L = 9.81 \times 10^{37} \text{ ergs s}^{-1}$. Here luminosity L was calculated from the relation $L = 4\pi d^2 F$, where F is the flux obtained from the spectral fits $3.28 \times 10^{-9} \text{ erg cm}^{-2} \text{ s}^{-1}$.

Substituting the above values for R_{disk} , $\alpha = 0.1$, and $\dot{m} = 5.28 \times 10^{17} \text{ g s}^{-1}$ based on the spectral fits, we found for lags 252 s and 817 s, the coronal height to be 3.28 km ($\beta = 0.01$), 16.43 km ($\beta = 0.05$), 32.86 km ($\beta = 0.1$) and 11.02 km ($\beta = 0.01$), 55.10 km ($\beta = 0.05$), 110.20 km ($\beta = 0.1$) respectively. While the lags of 138 s and 470 s were calculated to be 1.72 km ($\beta = 0.01$), 8.62 km ($\beta = 0.05$), 17.25 km ($\beta = 0.1$), and 6.27 km ($\beta = 0.01$), 31.35 km ($\beta = 0.05$), 62.70 km ($\beta = 0.1$) respectively.

We adopted another method to find the radius of the inner disk. Verdhan Chauhan et al. (2017) reported kHz QPO of about 850 Hz in 4U1728-34 using the AstroSat data. we used the following equation to get the radius (Wang et al. 2018)

$$r = 18.8 \text{ (km)} \left(\frac{M}{1.6M_{\odot}} \right)^{1/3} \left(\frac{v_2}{900 \text{ Hz}} \right)^{-2/3} \tag{2}$$

The above equation assumes that the kHz QPO is produced from the inner disc radius of the keplerian portion of the disc. Substituting the values for M and v_2 we found $r =$

18.67 km. This value is close to the value estimated from the spectra in the present study.

Substituting the above values for R_{disk} , $\alpha = 0.1$, and $\dot{m} = 5.28 \times 10^{17} \text{ g s}^{-1}$ based on the spectral fits, we found for lags 252 s and 817 s, the coronal height to be 3.02 km ($\beta = 0.01$), 15.14 km ($\beta = 0.05$), 30.28 km ($\beta = 0.1$) and 10.23 km ($\beta = 0.01$), 51.17 km ($\beta = 0.05$), 102.35 km ($\beta = 0.1$) respectively. The lag of 138 s and 470 s was calculated to be 1.57 km ($\beta = 0.01$), 7.86 km ($\beta = 0.05$), 15.73 km ($\beta = 0.1$), and 5.80 km ($\beta = 0.01$), 29.04 km ($\beta = 0.05$), 58.09 km ($\beta = 0.1$) respectively. Based on NuStar spectral data Wang et al. (2017) reported the presence of a compact corona in an atoll source 4U 1636-53 above the NS at a height of 2-3 R_g assuming a lamp-post model (García et al. 2014; Dauser et al. 2016). Since the height is low, they argued that this illuminating source could be associated with the boundary layer over the NS surface.

As it can be observed that some of our values of coronal height are low <5-6 km but others are relatively higher for higher values of β . Such a low height was reported by Wang et al. (2017) in an atoll source 4U 1636-53. They showed that the corona must be at a height of $h = 2-3 R_g$ to explain the X-ray spectral continuum.

5.2 Possible association of lags to boundary layer

Since these lags can be caused by the changing size of the boundary layer (BL), we used the formula to calculate its size Popham and Sunyaev (2001),

$$\log(R_{BL} - R_{NS}) \sim 5.02 + 0.245 \left[\log \left(\frac{\dot{M}}{10^{-9.85} M_{\odot} \text{ yr}^{-1}} \right) \right]^{2.19} \tag{3}$$

here \dot{M} is obtained from the equation $L = \frac{GM\dot{M}}{R}$ with $M = 1.4M_{\odot}$ and $R = 10$ km. The luminosity is obtained from the spectral fit (Table 4). The values of R_{BL} were determined to be 10.64 km for orbit 02393, 10.59 km for orbit 02394, and 10.61 km for orbit 02396. The BL size is similar to a few of the estimated coronal sizes and indicates that the lag could be due to structural variation associated with the BL which is acting like a corona. As the material from the disc falls onto the surface of the NS, it loses the angular velocity in order to match the angular velocity of the NS and eventually the material settles down over the surface forming a boundary layer. There are two timescales that are important during the phenomenon i.e. depletion and frictional time scale (Abolmasov et al. 2020; Abolmasov and Poutanen 2021). The depletion time scale is a characteristic time during which material replenishes or depletes in the boundary layer or spreading layer (SL) and the friction time scale is a time scale where the BL and NS angular velocity tries to

get into the equilibrium i.e. $\Omega = \Omega_{NS}$. It was shown that the friction and depletion time scales are much longer than the dynamical and viscous time scales in the inner region of the disc (Abolmasov and Poutanen 2021). These time scales are connected by the following equation $t_{depl}/t_{fric} = \alpha \Omega_K t_{depl}$ where α is a proportionality constant between the stress and pressure terms which is of the order of 10^{-6} to 10^{-7} and Ω_K is the Keplerian frequency (see equation (2) of Abolmasov and Poutanen (2021)). They have shown that for $\alpha = 10^{-7}$ the depletion time scale is $t_{depl} = 740$ s and it is lower for $\alpha = 10^{-6}$. These time scales are well in agreement with the observed lags seen in this source and other atoll sources. Overall the structural changes in the boundary layer can be associated with the lags.

The t_{depl} depends on rotation frequency as $t_{depl} = (\Omega - \Omega_{NS})/\alpha(\Omega_K^2 - \Omega^2)$, where $\Omega_K = \frac{1}{2\pi}\sqrt{GM_{NS}/R^3}$ (Abolmasov and Poutanen 2021) and $\Omega_{NS} = 363$ Hz (Verdhan Chauhan et al. 2017). For $R_{NS} = 10$ km of neutron star radius, $\Omega_K = 2169.44$ Hz, $\Omega = 767.01$ Hz for the material orbiting at a radius of $R = 20$ km, we get $t_{depl} = 98.10$ s ($\alpha = 10^{-6}$) and $t_{depl} = 981.05$ s ($\alpha = 10^{-7}$), $\Omega = 712.88$ Hz for $R = 21$ km, we get $t_{depl} = 83.34$ s ($\alpha = 10^{-6}$) and $t_{depl} = 833.40$ s ($\alpha = 10^{-7}$), $\Omega = 664.83$ Hz for $R = 22$ km, we get $t_{depl} = 70.77$ s ($\alpha = 10^{-6}$) and $t_{depl} = 707.79$ s ($\alpha = 10^{-7}$).

For a higher neutron star radius $R_{NS} = 15$ km, $\Omega_K = 1180.89$ Hz, $\Omega = 767.01$ Hz for $R = 20$ km, we get $t_{depl} = 501.13$ s ($\alpha = 10^{-6}$) and $t_{depl} = 5011.31$ s ($\alpha = 10^{-7}$), $\Omega = 712.88$ Hz for $R = 21$ km, we get $t_{depl} = 394.76$ s ($\alpha = 10^{-6}$) and $t_{depl} = 3947.66$ s ($\alpha = 10^{-7}$), $\Omega = 664.83$ Hz for $R = 22$ km, we get $t_{depl} = 316.88$ s ($\alpha = 10^{-6}$) and $t_{depl} = 3168.85$ s ($\alpha = 10^{-7}$). These time scales are well in agreement with the detected lags in 4U 1728-34 and hence can be associated with the depletion time scale of the BL.

Moreover, during this soft state, the inner disc is always close to the last stable orbit and the detected lags cannot be due to variation in the inner disc radius. We noted that all the detected lags are of different timescales indicating that illuminating source changes its structure possibly due to accreting material at varying latitudes over the NS surface contributing to the BL structure. The exact nature of the illuminating source i.e. corona or a boundary layer is still not understood in the atoll and Z sources and high-resolution X-ray observations are required to discern the nature of the source.

6 Conclusions

Using the AstroSat LAXPC data, we detected hard and soft lags of the order of a few hundred seconds in the banana/soft state of an atoll source 4U 1728-34. We confirm the significance of the lags based on simulations. Previous studies based on Astrosat data for atoll source viz. 4U 1705-44

clearly displayed hard and soft lags in its banana state, which were interpreted as readjustment time scales of corona in the inner region of the accretion disk. In the present study, the X-ray spectra were fitted with multi-component models, and the inner disc radius was found to be close to the NS surface. A reflection model was also used to unfold the spectra which resulted in the inner disc radius of ~ 16 km along with the presence of a low-temperature corona. We estimated the size of the corona height which was found to be low i.e. < 6 km for lower β values and higher for higher β values. The low coronal height cannot be ruled out because such values are observed in 4U 1636-53 (Wang et al. 2017). This indicates that the boundary layer around the NS surface can act as an illuminating source responsible for emitting the X-ray spectrum in a soft state. We show that the observed lags could be the depletion time scales of the boundary layer. Overall, the detected lags plausibly are readjustment time scales during which the boundary layer or low-temperature corona varies even when the inner disc radius is close to the last stable orbit. Future observations of 4U 1728-34 from AstroSat and Nustar along the various phases of HID would be helpful in understanding the lags and how the geometry of the boundary layer or corona is responsible for the observed lags.

Acknowledgements We thank the Referee for providing comments that improved the understanding of the paper. PC and KS acknowledge the Indian Space Research Organization (ISRO) for providing financial support under the AstroSat archival data utilization program. MS acknowledges INSPIRE program under DST, Govt. of India. VKA thanks GH, SAG; DD, PDMSA, and Director URSC for their encouragement and continuous support to carry out this research. This publication uses the data from the AstroSat mission of the Indian Space Research Organization (ISRO), archived at the Indian Space Science Data Center (ISSDC). This work uses the data from the LAXPC Instruments developed at TIFR, Mumbai, and the LAXPC-POC at TIFR is thanked for verifying and releasing the data. We also thank the AstroSat Science Support Cell hosted by IUCAA and TIFR for providing the LAXPCSOFT software to analyze the LAXPC data.

Author contributions PC and KS did the analysis and wrote the paper MS and VKA contributed to the idea and provided the logistics

Data Availability Data underlying this article are available at AstroSat-ISSDC website (https://astrobrowse.issdc.gov.in/astro_archive/archive/Home.jsp).

Declarations

Competing interests The authors declare no competing interests.

References

- Abolmasov, P., Poutanen, J.: *Astron. Astrophys.* **647**, 45 (2021)
- Abolmasov, P., Nättilä, J., Poutanen, J.: *Astron. Astrophys.* **638**, 142 (2020)
- Agrawal, P., Yadav, J., Antia, H., Dedhia, D., Shah, P., Chauhan, J.V., Manchanda, R., Chitnis, V., Gujar, V., Katoch, T., et al.: *J. Astrophys. Astron.* **38**(2), 1 (2017)

- Antia, H., Yadav, J., Agrawal, P., Chauhan, J.V., Manchanda, R., Chitnis, V., Paul, B., Dedhia, D., Shah, P., Gujar, V., et al.: *Astrophys. J. Suppl. Ser.* **231**(1), 10 (2017)
- Babkovskaia, N., Brandenburg, A., Poutanen, J.: *Mon. Not. R. Astron. Soc.* **386**(2), 1038 (2008)
- Basinska, E.M., Lewin, W.H.G., Sztajno, M., Cominsky, L.R., Marshall, F.J.: *Astrophys. J.* **281**, 337 (1984)
- Bhattacharyya, S., Yadav, J.S., Sridhar, N., Verdhan Chauhan, J., Agrawal, P.C., Antia, H.M., Pahari, M., Misra, R., Katoch, T., Manchanda, R.K., Paul, B.: *Astrophys. J.* **860**(2), 88 (2018)
- Chiranjeevi, P., Sriram, K.: *Mon. Not. R. Astron. Soc.* **516**(2), 2500 (2022)
- Dauser, T., García, J., Walton, D.J., Eikmann, W., Kallman, T., McClintock, J., Wilms, J.: *Astron. Astrophys.* **590**, 76 (2016)
- Di Salvo, T., Iaria, R., Burderi, L., Robba, N.R.: *Astrophys. J.* **542**(2), 1034 (2000)
- Egron, E., di Salvo, T., Burderi, L., Papitto, A., Barragán, L., Dauser, T., Wilms, J., D’Ai, A., Riggio, A., Iaria, R., Robba, N.R.: *Astron. Astrophys.* **530**, 99 (2011)
- Galloway, D.K., Psaltis, D., Chakrabarty, D., Muno, M.P.: *Astrophys. J.* **590**(2), 999 (2003)
- Galloway, D.K., Muno, M.P., Hartman, J.M., Psaltis, D., Chakrabarty, D.: *Astrophys. J. Suppl. Ser.* **179**(2), 360 (2008)
- Galloway, D.K., Yao, Y., Marshall, H., Misanovic, Z., Weinberg, N.: *Astrophys. J.* **724**(1), 417 (2010). <https://doi.org/10.1088/0004-637X/724/1/417>
- García, J., Dauser, T., Lohfink, A., Kallman, T.R., Steiner, J.F., McClintock, J.E., Brenneman, L., Wilms, J., Eikmann, W., Reynolds, C.S., Tombesi, F.: *Astrophys. J.* **782**(2), 76 (2014)
- Gilfanov, M., Revnivtsev, M., Molkov, S.: *Astron. Astrophys.* **410**(1), 217 (2003)
- Hasinger, G., van der Klis, M.: *Astron. Astrophys.* **225**, 79 (1989)
- Hoffman, J.A., Lewin, W.H.G., Doty, J., Hearn, D.R., Clark, G.W., Jernigan, G., Li, F.K.: *Astrophys. J. Lett.* **210**, 13 (1976)
- Kubota, A., Tanaka, Y., Makishima, K., Ueda, Y., Dotani, T., Inoue, H., Yamaoka, K.: *Publ. Astron. Soc. Jpn.* **50**(6), 667 (1998)
- Kubota, A., Makishima, K., Ebisawa, K.: *Astrophys. J.* **560**(2), 147 (2001)
- Lei, Y.J., Qu, J.L., Song, L.M., Zhang, C.M., Zhang, S., Zhang, F., Wang, J.M., Li, Z.B., Zhang, G.B.: *Astrophys. J.* **677**(1), 461 (2008)
- Lei, Y.-J., Zhang, H.-T., Zhang, C.-M., Qu, J.-L., Yuan, H.-L., Dong, Y.-Q., Zhao, Y.-H., Wang, D.-H., Yin, H.-X., Zhang, Y.-X., Song, L.-M.: *Astron. J.* **146**(3), 60 (2013)
- Lei, Y.-J., Zhang, S., Qu, J.-L., Yuan, H.-L., Wang, Y.-N., Dong, Y.-Q., Zhang, H.-T., Li, Z.-B., Zhang, C.-M., Zhao, Y.-H.: *Astron. J.* **147**(3), 67 (2014)
- Malu, S., Harikrishna, S., Sriram, K., Agrawal, V.K.: *Astrophys. Space Sci.* **366**(9), 1 (2021b)
- Malu, S., Sriram, K., Harikrishna, S., Agrawal, V.K.: *Mon. Not. R. Astron. Soc.* **506**(4), 6203 (2021a)
- Manmoto, T., Mineshige, S., Kusunose, M.: *Astrophys. J.* **489**(2), 791 (1997)
- Maoz, D., Netzer, H.: *Mon. Not. R. Astron. Soc.* **236**(1), 21 (1989)
- McKinney, J.C., Tchekhovskoy, A., Blandford, R.D.: *Mon. Not. R. Astron. Soc.* **423**(4), 3083 (2012)
- Mondal, A.S., Pahari, M., Dewangan, G.C., Misra, R., Raychaudhuri, B.: *Mon. Not. R. Astron. Soc.* **466**(4), 4991 (2017)
- Ng, C., Trigo, M.D., Bel, M.C., Migliari, S.: *Astron. Astrophys.* **522**, A96 (2010)
- Pen, U.-L., Matzner, C.D., Wong, S.: *Astrophys. J.* **596**(2), 207 (2003)
- Piraino, S., Santangelo, A., Kaaret, P.: *Astron. Astrophys.* **360**, 35 (2000)
- Popham, R., Sunyaev, R.: *Astrophys. J.* **547**(1), 355 (2001)
- Psaltis, D., Belloni, T., van der Klis, M.: *Astrophys. J.* **520**(1), 262 (1999)
- Revnivtsev, M.G., Gilfanov, M.R.: *Astron. Astrophys.* **453**(1), 253 (2006)
- Seifina, E., Titarchuk, L.: *Astrophys. J.* **738**(2), 128 (2011)
- Shakura, N.I., Sunyaev, R.A.: *Astron. Astrophys.* **24**, 337 (1973)
- Shaposhnikov, N., Titarchuk, L., Haberl, F.: *Astrophys. J. Lett.* **593**(1), 35 (2003)
- Shimura, T., Takahara, F.: *Astrophys. J.* **445**, 780 (1995)
- Sleator, C.C., Tomsick, J.A., King, A.L., Miller, J.M., Boggs, S.E., Bachetti, M., Barret, D., Chenevez, J., Christensen, F.E., Craig, W.W., Hailey, C.J., Harrison, F.A., Rahoui, F., Stern, D.K., Walton, D.J., Zhang, W.W.: *Astrophys. J.* **827**(2), 134 (2016)
- Sriram, K., Agrawal, V., Pendharkar, J.K., Rao, A.: *Astrophys. J.* **661**(2), 1055 (2007)
- Sriram, K., Choi, C., Rao, A.: *Astrophys. J. Suppl. Ser.* **200**(2), 16 (2012)
- Sriram, K., Malu, S., Choi, C.: *Astrophys. J. Suppl. Ser.* **244**(1), 5 (2019)
- Sriram, K., Chiranjeevi, P., Malu, S., Agrawal, V.: *J. Astrophys. Astron.* **42**(2), 1 (2021)
- Strohmayer, T.E., Zhang, W., Swank, J.H., Smale, A., Titarchuk, L., Day, C., Lee, U.: *Astrophys. J.* **469**(1), 9 (1996)
- Tarana, A., Belloni, T., Bazzano, A., Méndez, M., Ubertini, P.: *Mon. Not. R. Astron. Soc.* **416**(2), 873 (2011)
- van der Klis, M.: In: *X-Ray Binaries*, p. 252 (1995)
- van der Klis, M.: In: Strohmayer, T.E. (ed.) *Rossi2000: Astrophysics with the Rossi X-Ray Timing Explorer* (2000)
- van der Klis, M.: A review of rapid X-ray variability in X-ray binaries (2004). [arXiv:astro-ph/0410551](https://arxiv.org/abs/astro-ph/0410551)
- Verdhan Chauhan, J., Yadav, J.S., Misra, R., Agrawal, P.C., Antia, H.M., Pahari, M., Sridhar, N., Dedhia, D., Katoch, T., Madhwani, P., Manchanda, R.K., Paul, B., Shah, P.: *Astrophys. J.* **841**(1), 41 (2017)
- Wang, Y., Méndez, M., Sanna, A., Altamirano, D., Belloni, T.M.: *Mon. Not. R. Astron. Soc.* **468**(2), 2256 (2017)
- Wang, D.-H., Zhang, C.-M., Qu, J.-L.: *Astron. Astrophys.* **618**, 181 (2018)
- Wang, Y., Méndez, M., Altamirano, D., Zhang, G., Belloni, T.M., Ribeiro, E.M., Linares, M., Sanna, A., Motta, S.E., Tomsick, J.A.: *Mon. Not. R. Astron. Soc.* **484**(3), 3004 (2019)
- Wijnands, R., van der Klis, M.: *Astrophys. J.* **514**(2), 939 (1999)
- Yadav, J., Agrawal, P., Antia, H., Chauhan, J.V., Dedhia, D., Katoch, T., Madhwani, P., Manchanda, R., Misra, R., Pahari, M., et al.: In: *Space Telescopes and Instrumentation 2016: Ultraviolet to Gamma Ray*, vol. 9905, p. 374. SPIE, Bellingham (2016)

Publisher's Note Springer Nature remains neutral with regard to jurisdictional claims in published maps and institutional affiliations.

Springer Nature or its licensor (e.g. a society or other partner) holds exclusive rights to this article under a publishing agreement with the author(s) or other rightsholder(s); author self-archiving of the accepted manuscript version of this article is solely governed by the terms of such publishing agreement and applicable law.